Detection and Mitigation of Ground Clutter in Polarimetric Phased Array Radar Measurements Using Machine Learning and Physics-based Discriminants

Zhe Li, Guifu Zhang, and Yuechen Wu

Abstract— This paper presents clutter detection and mitigation for polarimetric phased array weather radar measurements using machine learning. The following three approaches are analyzed for clutter detection in the cylindrical polarimetric phased array radar measurements, including naive Bayes classifier (NBC), multilayer perceptron (MLP), and convolutional neural network (CNN). Results show that CNN achieves the best performance in clutter detection, followed by MLP and NBC. This is because CNN utilizes spatial information of the input images, which has different features for clutter from that for weather. It is also shown that the combination of physics-based discriminants of power ratio and raw radar measurements is more effective in clutter detection than the direct use of raw radar measurements. In addition, CNN is employed for clutter mitigation and its performance is compared with the traditional speckle filter technique. It is demonstrated that CNN outperforms the speckle filter and incorporation of power ratio in the training process could further improve CNN's performance in clutter mitigation.

Index Terms— Clutter detection and mitigation, machine learning, multilayer perceptron, convolutional neural network, polarimetric phased array radar.

I. Introduction

In weather radar observations, ground clutter is a major source of measurement error that degrades radar data quality. Generally, ground clutter refers to the non-weather echoes from stationary objects on the ground, characterized by a nearly zero Doppler velocity and a narrow spectrum width. Therefore, it is desirable to identify clutter and minimize its impact on weather measurements. Over the past several decades, a range of clutter detection and mitigation techniques have been suggested and implemented.

Previously, a static clutter map derived from clear-air conditions was utilized to identify the range gates contaminated by ground clutter [1]. However, this method does not work well in case of variable clutter and anomalous propagation, highlighting the need for a more flexible clutter detection

algorithm. To adjust to variable clutter, the clutter mitigation decision (CMD) was introduced by Hubbert et al. [2-3]. CMD is a fuzzy logic algorithm for automatic clutter detection based on clutter phase alignment (CPA) and local texture information. Realizing the different polarimetric and statistical properties of ground clutter and weather returns, Li et al. [4] suggested a simple Bayesian classifier with new discriminants for clutter detection. Recently, phased array radar (PAR) technology has attracted considerable attention in the weather radar community due to its rapid data updates and multi-mission capabilities through electronic scans. Li and Zhang [5] explored the similarities and differences in clutter detection using electronic scans and mechanical scans with a cylindrical polarimetric phased array radar (CPPAR) [6-7]. Also, Warde and Torres [8-9] presented the Clutter Environment Analysis using Adaptive Processing (CLEAN-AP) filter, which integrated ground clutter detection and mitigation using autocorrelation spectral density, and it is presently being evaluated on the Weather Surveillance Radar-1988 Doppler (WSR-88D). Despite being effective in clutter detection and mitigation, these existing methods employ either single gate radar measurements or empirically derived local texture information, which have limitations of not using all pertinent information in weather radar signals.

Lately, alongside conventional signal processing techniques, machine learning approaches have been investigated in the radar community due to their computational efficiency and adaptability. For example, Vicen-Bueno et al. [10] proposed a neural network-based clutter reduction system, which could achieve a good performance under different environmental conditions. Jatau et al. [11] introduced a machine learning classifier capable of detecting various patterns of bird and insect echoes based on dual-polarization variables at each range gate of WSR-88D. More recently, Kim and Cheong [12] proposed a convolutional neural network-based algorithm to deal with the velocity dealiasing issue in weather radar, which achieved similar performance in regions mostly filled with precipitation and better performance in regions sparsely filled with precipitation compared to the traditional region-based method.

This work was partially supported by the National Science Foundation with the grant of AGS-2136161 and the National Oceanic and Atmospheric Administration (NOAA) under Grant NA16OAR4320115.

Zhe Li and Yuechen Wu are with the MathWorks, Natick, MA 01760 USA (e-mail: lizhe0906@gmail.com, ywu788@gmail.com).

Guifu Zhang is with the School of Meteorology, The University of Oklahoma, Norman, OK 73072 USA (e-mail: guzhang1@ou.edu).

Veillette et al. [13] presented a deep neural network that is used to emulate the 2-dimensional WSR-88D Open Radar Product Generator (ORPG) dealiasing algorithm, which is shown to be effective in building accurate, fast, and portable velocity dealiasing algorithms.

This work is motivated by the requirement for clutter detection and mitigation in PAR measurements and successful implementation of machine learning approaches in radar applications mentioned above. It presents clutter detection and mitigation results using machine learning with the CPPAR as shown in Fig.1. The remainder of this paper is organized as follows. Section II introduces datasets utilized in this study and defined input variables. Section III presents three machine learning techniques for clutter detection, including naive Bayes classifier (NBC), multilayer perceptron (MLP), convolutional neural network (CNN), whose performance are evaluated using actual CPPAR measurements in electronic scans. Section IV provides clutter mitigation results based on CNN with and without using power ratio, which are compared with the traditional speckle filter technique. Section V summarizes the results and conclusion.



Fig. 1. The CPPAR installed at the rooftop of the Radar Innovations Laboratory at the University of Oklahoma.

II. DATASETS AND INPUT VARIABLES

A. Datasets

The data used for this study were collected by the CPPAR. The CPPAR measurements consist of three spectral moments including reflectivity (Z_H) , radial velocity (v_r) , spectrum width $(\sigma_{\rm v})$, and three polarimetric variables including differential reflectivity (Z_{DR}) , copolar correlation coefficient (ρ_{hv}) , and differential phase (ϕ_{DP}) . Each of these radar variables is affected differently by ground clutter and by weather. Ground clutter has abrupt changes in $Z_{\rm H}$, close to zero $v_{\rm r}$, and very small $\sigma_{\rm v}$, while weather tends to have smooth features in $Z_{\rm H}$ and can have large $v_{\rm r}$ and $\sigma_{\rm v}$. The three polarimetric variables $(Z_{\rm DR},\,
ho_{
m hv},\,$ and $\phi_{
m DP})$ contain further information about the difference between clutter and weather. Z_{DR} is a measure of the reflectivity difference between horizontally and vertically polarized waves, which has a larger spatial variation for clutter than that for weather. ρ_{hv} represents the similarity between horizontal and vertical polarization signals, which is reduced when there is random differential backscattering phase in the signals, which is usually caused by non-Rayleigh scattering and non-spherical scatterers with random motion and orientation in the resolution volume. $\phi_{\rm DP}$ is the difference in phase shift between horizontally and vertically polarized waves, which has a larger variation for clutter than that for weather.

The CPPAR data were collected via electronic scans during the period from August 2019 to May 2020, which included a variety of weather and clutter measurements. To evaluate the performance of clutter detection and mitigation, 20 training datasets and 2 independent test datasets are employed, and each dataset refers to radar measurements (images) from one sector scan collected at a different time. The training data serves to train the machine learning models, while the test data aims to evaluate the efficacy of the trained models. Each training dataset consists of both pure clutter data and pure weather data. On one hand, pure clutter data was collected under clear air conditions using a 1 µs simple rectangular pulse, without applying a clutter filter to the received time series. To reduce the impact of noise, a clutter-to-noise ratio threshold of 5 dB was applied to the pure clutter data. Furthermore, only range gates with v_r and σ_v below 1 m/s were chosen to guarantee that the collected clutter measurements remained uncontaminated by moving objects like birds or aircrafts. On the other hand, pure weather data was acquired during precipitation events using a 34 µs nonlinear frequency modulation (NLFM) pulse compression waveform [7]. To minimize contamination from clutter and noise, weather measurements exceeding 20 km were selected, and a signal-to-noise ratio threshold of 5 dB was applied to the pure weather data.

As an example, one of the 20 training datasets is shown in Fig.2 to Fig.4, where Fig.2 is the image for pure weather measurements collected on 30 March 2020, Fig.3 is the image for pure clutter measurements collected on 9 May 2020, and Fig.4 is the image for composed measurements. Two test datasets include both convective and stratiform rain events. The first test dataset is composed of a convective rain collected on 15 May 2020 and clutter measurements on 30 May 2020. The second test dataset is compiled from a stratiform rain collected on 25 May 2020 and clutter measurements on 30 May 2020. The composed radar measurements of $Z_{\rm H}$, $v_{\rm r}$, $\sigma_{\rm v}$, $Z_{\rm DR}$, $\rho_{\rm hv}$, and $\phi_{\rm DP}$ for the two test cases are shown in Fig.5 and Fig.6, respectively.

To evaluate the clutter detection performance, ground truth clutter map is needed, which is generated by finding those gates where clutter significantly biases weather radar estimates. In this study, to be consistent with WSR-88D specifications for data quality, a resolution volume is considered to have weather signals contaminated by clutter only if ground clutter biases the weather signal's reflectivity estimates by more than 1 dB, or its radial velocity estimates by more than 1 m/s, or its spectrum width estimates by more than 1 m/s. Otherwise, even if ground clutter from a range bin is mixed with weather signal, the combined signal is still considered as weather signal because the clutter's effect on radar estimates can be neglected [4].

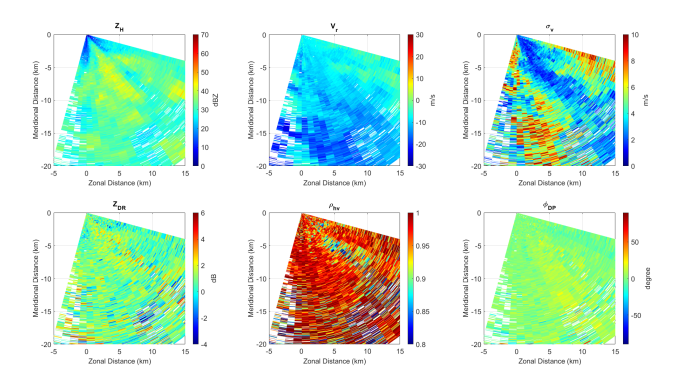


Fig. 2. The pure weather measurements of an example training dataset.

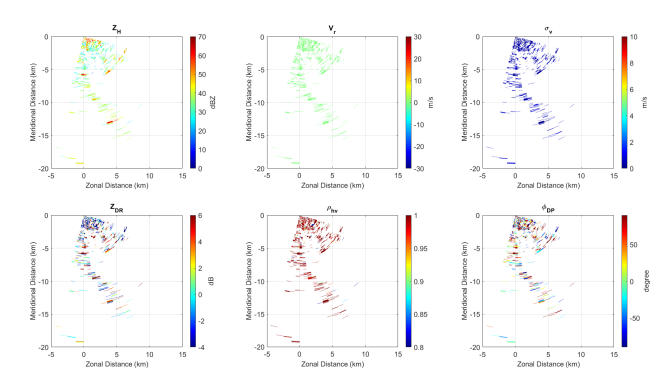


Fig. 3. The pure clutter measurements of an example training dataset.

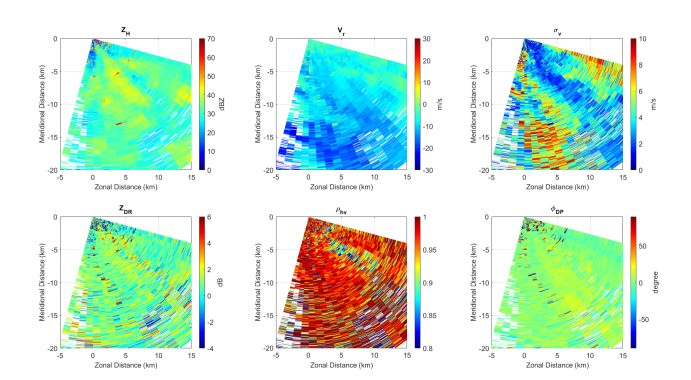


Fig. 4. The composed measurements of an example training dataset.

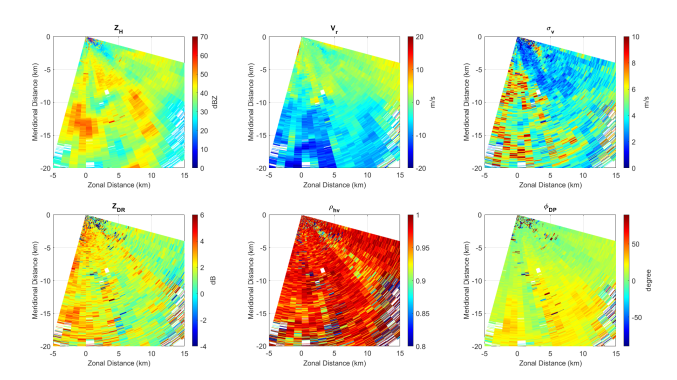


Fig. 5. The composed measurements of test case 1.

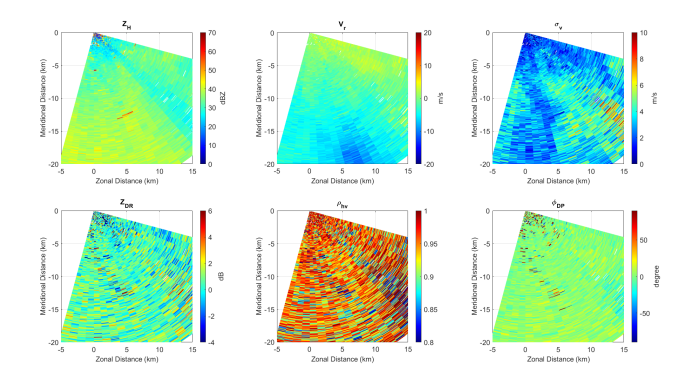


Fig. 6. The composed measurements of test case 2.

B. Input Variables and Discriminants

In this work, two sets of input variables are employed to evaluate the clutter detection and mitigation performance of machine learning techniques. The first set of input variables is comprised of 6 raw radar measurements of $Z_{\rm H}$, $v_{\rm r}$, $\sigma_{\rm v}$, $Z_{\rm DR}$, $\rho_{\rm hv}$, and ϕ_{DP} . The second set of input variables is made up of 8 radar estimates, which include not only the above 6 raw radar measurements, but also two power ratios (PR_H and PR_V) that have distinct property/value between clutter and weather as shown in section II-C of [5]. The power ratio (PR) is the ratio in decibels between coherent power and incoherent power as defined in section 5.4.2 of [14]. While radar signals from stationary ground clutter tend to be coherent, the signals from randomly distributed weather scatterers are incoherent. Therefore, the power ratio has a small value for weather that produces incoherent power, compared to a large value for ground clutter which is close to stationary and yields more coherent power. PR is estimated from polarimetric radar signals as follows:

$$\widehat{PR}_{H,V} = 10\log_{10} \left[\frac{\left| \frac{1}{M} \sum_{m=1}^{M} V_{h,v}(m) \right|^{2}}{\left| \frac{1}{M} \sum_{m=1}^{M} \left| V_{h,v}(m) \right|^{2} - \left| \frac{1}{M} \sum_{m=1}^{M} V_{h,v}(m) \right|^{2}} \right]$$
(1)

where $V_{\rm h,v}$ represents complex voltage samples for each range gate in horizontal or vertical polarization, M is the number of samples in the dwell time. As \widehat{PR}_H and \widehat{PR}_V provide additional information, their combination with raw radar measurements yields a set of 8 input variables which are PR_H , PR_V , Z_H , v_r , σ_v , $Z_{\rm DR}$, $\rho_{\rm hv}$, and $\phi_{\rm DP}$, allowing a further separation between weather and ground clutter.

III. CLUTTER DETECTION

A. Naive Bayes Classifier

With a naive Bayes classifier (NBC), radar returns can be divided into two categories: ground clutter (c) and weather signal (w). Taking 8 input variables for example, in each range gate, $x = x^0 = (PR_H^0, PR_V^0, Z_H^0, v_r^0, \sigma_v^0, Z_{DR}^0, \rho_{hv}^0, \phi_{DP}^0)$, where x represents the discriminant vector, and the superscript "O" means the observation. The NBC assigns $x = x^0$ to c only if $p(c|x = x^0) > p(w|x = x^0)$, where p refers to the posterior

probability. According to the Bayes' theorem [4], $p(i|x=x^0)$ is proportional to $p(x=x^0|i)$ (i=c or w), so the NBC assigns the observation $x=x^0$ to c only if $p(x=x^0|c) > p(x=x^0|w)$. Different from the Bayes classifier utilized in [4-5] which includes the partial dependence, the NBC makes a naive assumption of class-conditional independence, which enables fast and efficient calculation of the probabilities.

$$p(x = x^{o}|i) = p(PR_{H} = PR_{H}^{o}|i) \times p(PR_{V} = PR_{V}^{o}|i)$$

$$\times p(Z_{H} = Z_{H}^{o}|i) \times p(v_{r} = v_{r}^{o}|i) \times p(\sigma_{v} = \sigma_{v}^{o}|i)$$

$$\times p(Z_{DR} = Z_{DR}^{o}|i) \times p(\rho_{hv} = \rho_{hv}^{o}|i) \times p(\phi_{DP} = \phi_{DP}^{o}|i)$$
(2)

B. Multilayer Perceptron

The multilayer perceptron (MLP) is a fully connected multilayer neural network that maps a set of input variables to the output [15], as shown in Fig.7. The MLP's output y is determined by the weighted sum of the input variables v = $\varphi(wx + b)$, where x is the input variables (discriminant vector), w is the weights, b is the bias term, and φ is the activation function. In this study, softmax function is employed as the activation function of the output node, $y_1 = \varphi(v_1) =$ $e^{v_1}/(e^{v_1}+e^{v_2})$, $y_2=\varphi(v_2)=e^{v_2}/(e^{v_1}+e^{v_2})$, where v_i is the weighted sum of the i-th output node (i = 1, 2). In practice, softmax function is the most widely used activation function for classification neural networks. Taking 8 input variables for example, $PR_{\rm H}$, $PR_{\rm V}$, and 6 raw radar measurements are utilized as input variables to the MLP. Two hidden layers with a size of 16 are adopted. The model generates output labels that classify the return at each range gate as being from clutter or weather. The scaled conjugate gradient algorithm is employed to train the MLP model iteratively updating network weight and bias values until a satisfactory solution or local optimum is reached. In contrast to NBC, which simply assumes independence among input variables, MLP accounts for the correlations and joint probability of the input variables. However, it should be noted that both NBC and MLP deal with the measurements at a single range gate without including the spatial correlation information.

C. Convolutional Neural Network

The convolutional neural network (CNN) is a type of deep neural network specifically designed for image recognition [15]. Different from MLP, CNN employs the convolution layer containing a set of filters (kernels) to convert input images into feature maps that accentuate the unique features of the input images. Each filter of the convolution layer is a two-dimensional matrix with values determined through the training process. The feature maps generated by the convolution layer are further processed through the activation function which usually employs the rectified linear unit (ReLU) y = max(0,x). In this work, the CNN network is designed using MATLAB Deep Learning Toolbox [16]. Also taking 8 input

variables for example, the input layer contains 8 channels, each with a size of 25 x 800, where 25 is the number of azimuths and 800 is the number of range gates in each image. Additionally, a batch normalization layer is inserted between the convolutional layer and ReLU layer. This layer normalizes the activations from the previous layer by computing the mean and variance of each feature within the mini-batch data, followed by scaling and shifting the normalized values using learned parameters. This process helps to accelerate training, increases the model's robustness to network initialization, and reduces internal covariate shift. Out of the 20 training datasets, 16 datasets are used for training and the remaining 4 serve as validation data for fine-tuning the CNN model parameters. The Adam algorithm is used to train the CNN model, which utilizes the moving averages to update the network weights. The CNN network architecture is shown in Fig.8, with a description of each layer in Table I.

TABLE I
CNN NETWORK ARCHITECTURE FOR CLUTTER DETECTION

Layer Number	Layer Name	Description
1	Input Layer	Input size: 25 x 800 x 8
2	Convolution Layer	8 filters each with a size of 3 x 3
3	Batch Normalization Layer	Batch normalization
4	ReLU Layer	ReLU activation function
5	Convolution Layer	4 filters each with a size of 3 x 3
6	Batch Normalization Layer	Batch normalization
7	ReLU Layer	ReLU activation function
8	Convolution Layer	2 filters each with a size of 3 x 3
9	Batch Normalization Layer	Batch normalization
10	ReLU Layer	ReLU activation function
11	Convolution Layer	2 filters each with a size of 3 x 3
12	Softmax Layer	Softmax activation function
13	Classification Layer	Output size: 25 x 800

D. Results and Evaluation

For a quantitative evaluation of the clutter detection performance, the probability of detection (POD), probability of false alarm (PFA), and critical success index (CSI) are calculated, which are defined as POD = TP/(TP + FN), PFA = FP/(FP + TN), and CSI = TP/(TP + FN + FP), where TP refers to "True Positive" (clutter detected as clutter), FN stands for "False Negative" (clutter detected as weather), FP refers to "False Positive" (weather detected as clutter), and TN stands for "True Negative" (weather detected as weather). The number of TP, FN, FP, TN, POD, PFA, and CSI for the two test cases based on the two sets of input variables using NBC, MLP, and CNN approaches are listed in Table II and Table III, respectively. Accordingly, the POD and CSI as a function of clutter-to-signal ratio (CSR) for the two test cases are plotted in Fig.9. In addition, the ground truth and detected clutter maps based on 8 input variables for the two test cases are plotted in Fig. 10 and Fig. 11, respectively.

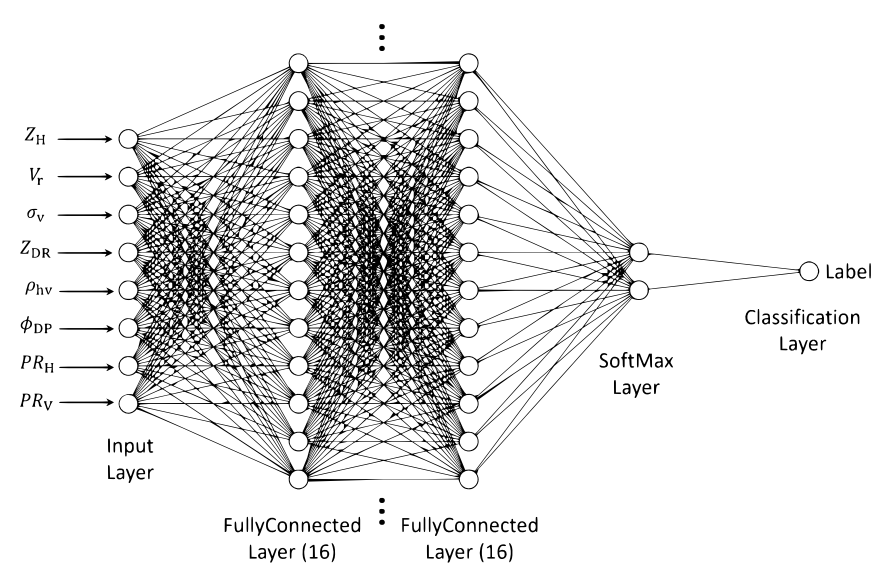
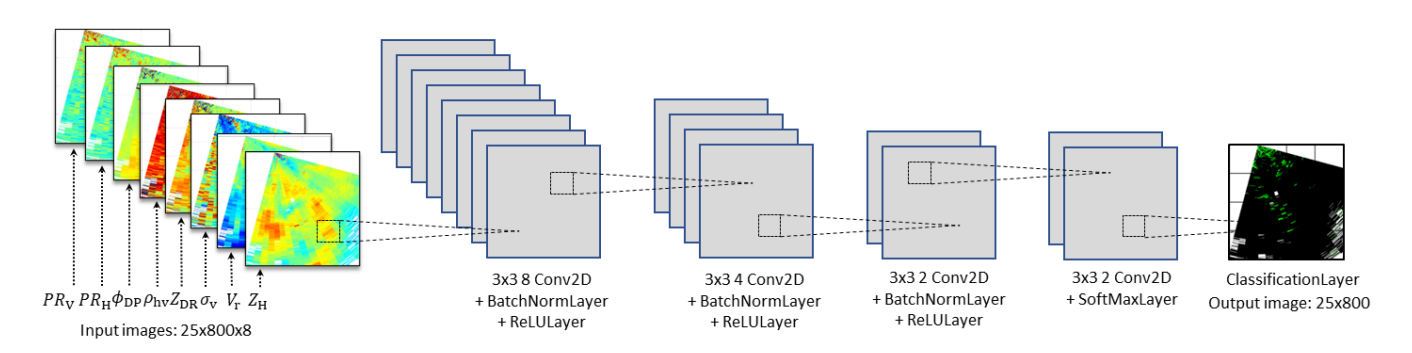


Fig. 7. The block diagram of MLP for clutter detection.



 $Fig.\ 8.\ CNN\ structure\ diagram\ for\ clutter\ detection.$

TABLE II CLUTTER DETECTION RESULTS OF TEST CASE 1

	NBC		MLP		CNN	
	NBC-6 (6 inputs)	NBC-8 (8 inputs)	MLP-6 (6 inputs)	MLP-8 (8 inputs)	CNN-6 (6 inputs)	CNN-8 (8 inputs)
TP	1062	1258	1164	1285	1241	1325
FN	338	142	236	115	159	75
FP	317	218	109	36	59	72
TN	17157	17256	17365	17438	17415	17402
POD	0.7586	0.8986	0.8314	0.9179	0.8864	0.9464
PFA	0.0181	0.0125	0.0062	0.0021	0.0034	0.0041
CSI	0.6185	0.7775	0.7714	0.8948	0.8506	0.9001

TABLE III

		CLUTTER D	DETECTION RESULTS OF	TEST CASE 2			
	N	NBC		MLP		CNN	
	NBC-6 (6 inputs)	NBC-8 (8 inputs)	MLP-6 (6 inputs)	MLP-8 (8 inputs)	CNN-6 (6 inputs)	CNN-8 (8 inputs)	
TP	1138	1382	1267	1379	1405	1432	
FN	361	117	232	120	94	67	
FP	65	127	49	68	31	40	
TN	18127	18065	18143	18124	18161	18152	
POD	0.7592	0.9219	0.8452	0.9199	0.9373	0.9553	
PFA	0.0036	0.0070	0.0027	0.0037	0.0017	0.0022	
CSI	0.7276	0.8499	0.8185	0.8800	0.9183	0.9305	

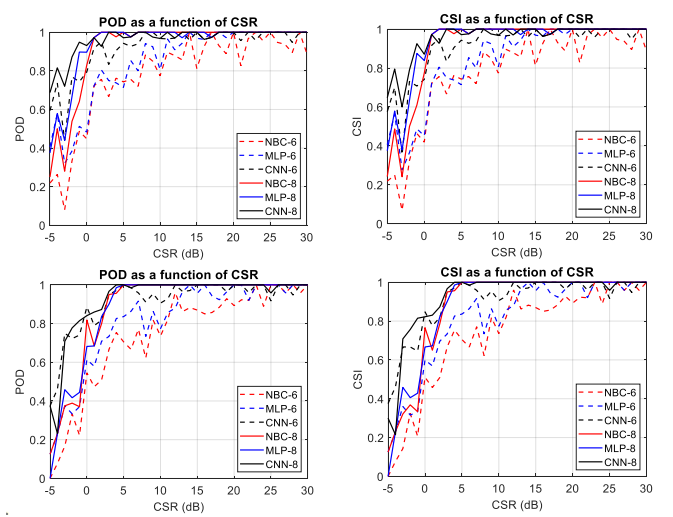


Fig. 9. The POD and CSI as a function of CSR based on 6 and 8 input variables using NBC, MLP, and CNN method, respectively. Top row: test case 1; bottom row: test case 2

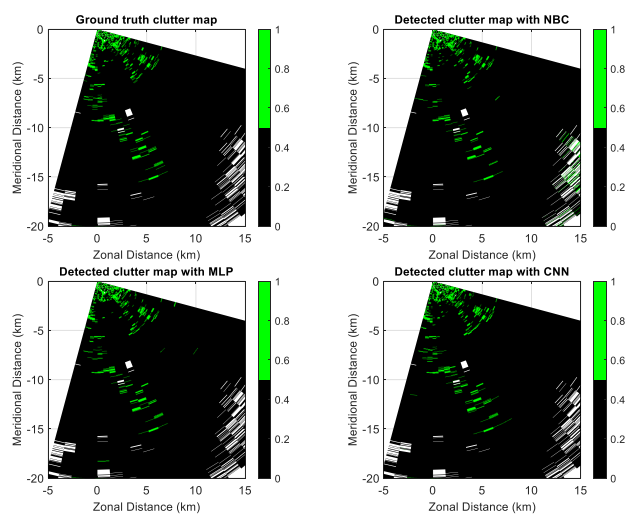


Fig. 10. The ground truth and detected clutter maps of test case 1 based on 8 discriminants using NBC, MLP, and CNN method, respectively.

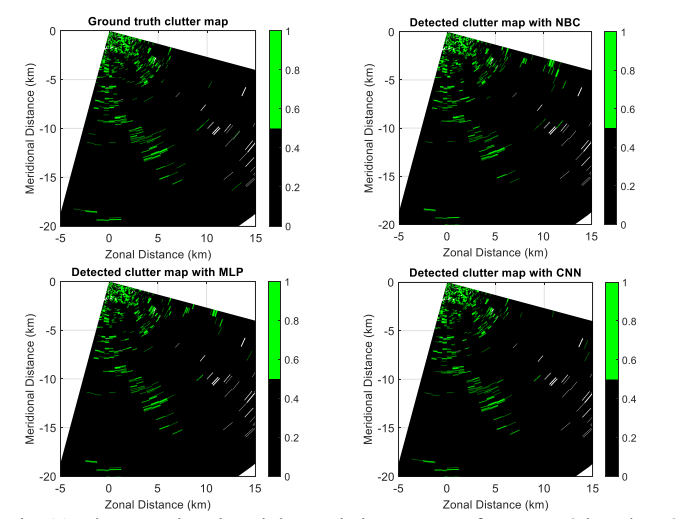


Fig. 11. The ground truth and detected clutter maps of test case 2 based on 8 discriminants using NBC, MLP, and CNN method, respectively.

As shown in Table II to Table III and Fig. 9 to Fig. 11, when 8 radar variables are employed as inputs, for both test cases, CNN achieves the best clutter detection performance among all the three machine learning approaches, especially in the lower CSR region. Specifically, CNN method has the highest POD and CSI as well as low PFA. A physical explanation is that CNN method utilizes spatial information of the input images, that is, weather returns have gate-to-gate continuity while clutter has gate-to-gate abrupt variations, which is helpful for detecting clutter from weather. In contrast, neither NBC nor MLP method uses any spatial information of the input variables. In addition, the test result shows MLP performs better than NBC. While they have similar POD, MLP achieves a lower PFA than NBC and thus a higher CSI. The reason is that NBC makes a naive assumption of class-conditional independence, which may not be valid in actual measurements with the CPPAR. As a comparison, MLP doesn't make such an assumption but instead generates a deep feedforward neural network to approximate the nonlinear function mapping the 8 input variables that can be correlated to the output category (clutter or weather). To some extent, MLP includes the correlation and joint probability of input variables and is more robust than NBC. Also, it is found that the POD of test case 2 is generally higher than that of test case 1 for all the three machine learning approaches, because test case 2 has a larger

Similarly, when only the 6 raw radar measurements are directly used as input variables without including $PR_{\rm H}$ and $PR_{\rm V}$, CNN achieves the best clutter detection performance, followed by MLP which performs better than NBC. By comparison, it is shown that the clutter detection based on 8 input variables performs better than that based on 6 input variables. The reason is that $PR_{\rm H}$ and $PR_{\rm V}$ characterize the ratio of coherent power and incoherent power which yields better separation between clutter and weather. Therefore, their combination with the 6 raw radar measurements allows for improved clutter detection, which demonstrates that an optimal selection of physics-based discriminants is desirable.

IV. CLUTTER MITIGATION

As CNN has shown an excellent performance in clutter detection, it is also employed for clutter mitigation in this study. Again, two sets of input variables are utilized to compare the clutter mitigation performance. For the first set of inputs, CNN's input layer contains six channels $(Z_{\rm H}, v_{\rm r}, \sigma_{\rm v}, Z_{\rm DR}, \rho_{\rm hv})$ and ϕ_{DP}), while the output is one of the six radar variables. Each CNN is trained to learn an effective nonlinear relationship between the six input radar variables and a corresponding output radar variable. As clutter mitigation is inherently a regression problem, a regression layer is adopted as the output layer. As before, the Adam algorithm is used to train each CNN model. On the other hand, for the second set of inputs, PR_H and PR_v along with six raw radar measurements are incorporated into the training process of each CNN to help improve the clutter mitigation performance, that is, each CNN network architecture efficiently maps all eight input radar variables to a single output radar variable. This approach leverages multiple

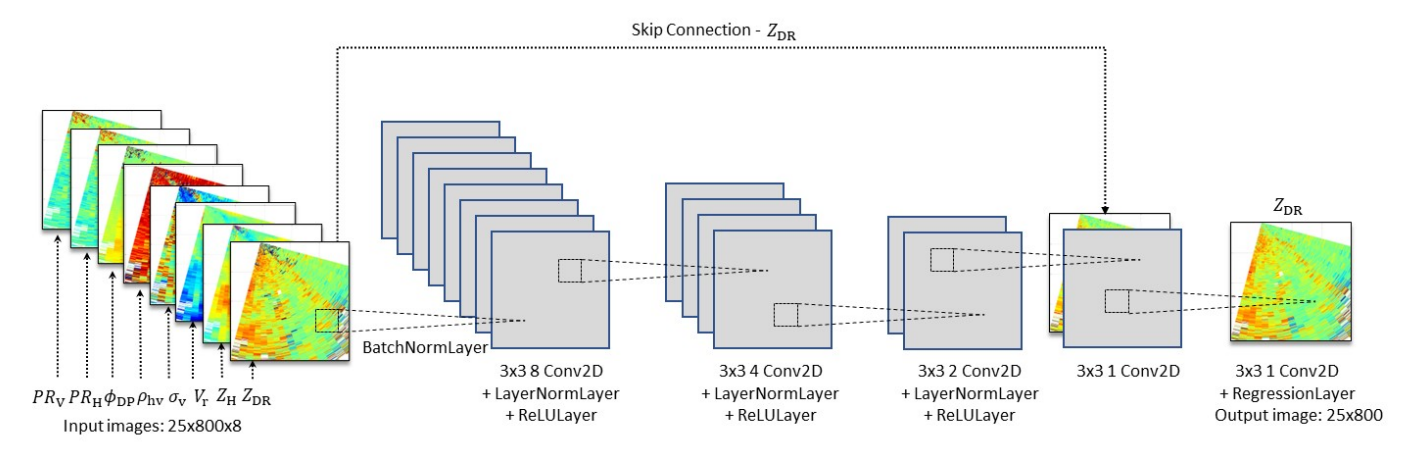


Fig. 12. CNN structure diagram for clutter mitigation, illustrated using $Z_{\rm DR}$ variable prediction as an example.

types of input information for the collaborative prediction of a specific radar variable, thereby enhancing overall performance. Fig. 12 illustrates the CNN structure diagram for clutter mitigation based on 8 input variables, using the prediction of $Z_{\rm DR}$ as an example. As shown in Fig.12, a skip connection is introduced, concatenating the original input of the target variable ($Z_{\rm DR}$) with the features extracted from multiple CNN layers near the output. This method enables the output to retain focus on the target variable while efficiently utilizing supplementary information.

The CNN input images of the two test cases are the same as Fig.5 and Fig.6, respectively. The expected truth images of the two test cases only contain pure weather data, as shown in Fig.13 and Fig.14, respectively. The actual CNN output images based on 6 input variables for the two test cases are shown in Fig. 15 and Fig. 16, respectively. As a comparison, CNN output images based on 8 input variables for the two test cases are shown in Fig. 17 and Fig. 18, respectively. As observed in Fig. 15 to Fig. 18, for both test cases, most of the clutter is removed, and the output images from CNN based on 8 input variables are visually closer to the expected truth images. Furthermore, for a quantitative evaluation of clutter mitigation performance, the root mean square error (RMSE) is calculated between CNN's output images and truth images for the two test cases, as presented in Table IV and Table V. It is shown that for each radar variable, the RMSE based on 8 input variables is lower than that based on 6 input variables. A possible explanation for this improvement is that PR_H and PR_V provide additional information about the clutter map, enabling the CNN to learn more effectively and enhancing clutter mitigation performance. Additionally, the local standard deviation (LSTD) of CNN's output based on 6 and 8 input variables is estimated and presented in Table VI and Table VII. As a baseline, estimated LSTD of the truth images (pure weather measurements) is also included. As documented in [7], the LSTD can be obtained from the median value of the corresponding histogram of each radar estimate. As shown in Table VI and Table VII, the LSTD of CNN's output based on 8 input variables is generally closer to the estimated LSTD of the truth images, which indicates the details of weather returns are better preserved.

Moreover, to compare the clutter mitigation performance of the CNN with the traditional radar image processing technique, speckle filter is utilized as a baseline [17-18]. As shown in Fig.5 and Fig.6, most of the weather returns are located between 10 km and 20 km. As the CPPAR has a wide beamwidth of around 6 degrees, due to the beam broadening effect, at the middle range of 15 km, the cross-range resolution is about 1.5 km. To make the radial range resolution comparable to the cross-range resolution, given the CPPAR has a range gate of 30 m, a moving average of 51 gates is used for speckle filtering along each azimuth (beam direction) of the input images. The output images from the speckle filter for the two test cases are shown in Fig.19 and Fig.20, respectively. As can be seen, although most of the clutter are removed by speckle filter, the spatial resolution of the output images is significantly degraded as a tradeoff, which indicates some finer details of weather returns are lost. As a quantitative assessment, the RMSE between speckle filter output and truth images for the two test cases is also included in Table IV and Table V, which shows that the RMSE of speckle filter is larger than that of CNN for each radar variable. Additionally, the LSTD of speckle filter's output for the two test cases is also presented in Table VI and Table VII, respectively. For a fair comparison, the LSTD is also obtained from radar estimates over 51 gates in each beam direction. As can be seen, due to the smoothing effect, the LSTD of speckle filter's output is much lower than the estimated LSTD of the truth images for each radar variable, indicating undesirable image distortion introduced by speckle filtering.

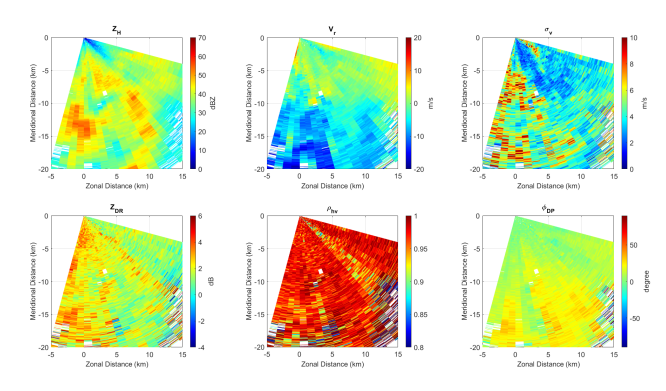


Fig. 13. Expected truth images of test case 1.

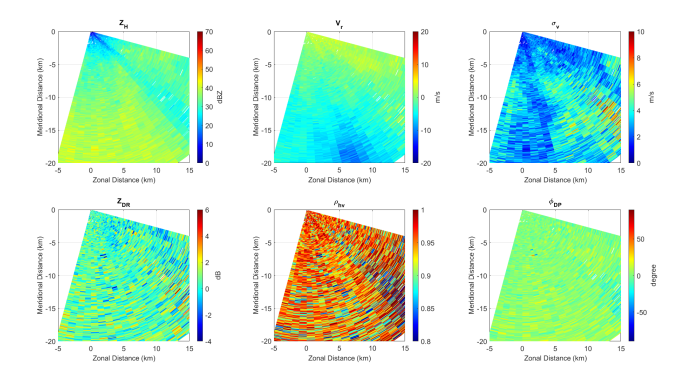


Fig. 14. Expected truth images of test case 2.

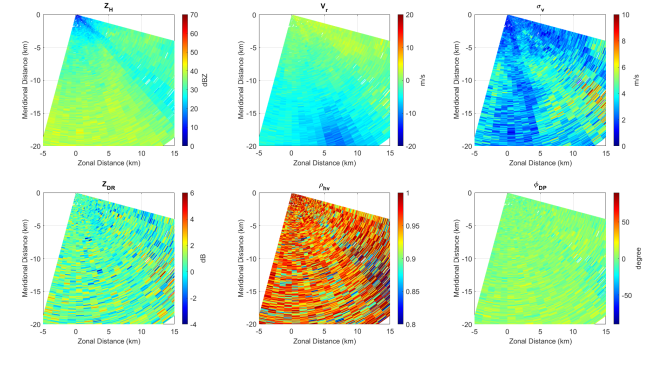


Fig. 18. Actual output images from CNN using 8 input variables of test case 2.

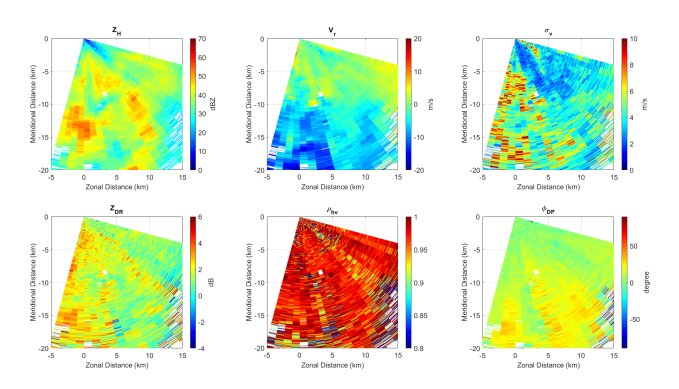


Fig. 15. Actual output images from CNN using 6 input variables of test case 1.

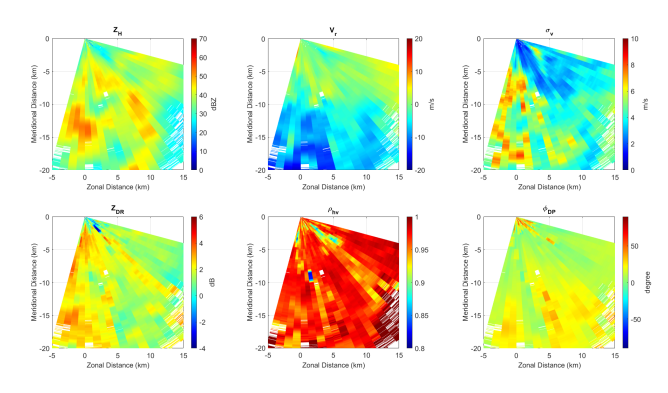


Fig. 19. Actual output images from speckle filter of test case 1.

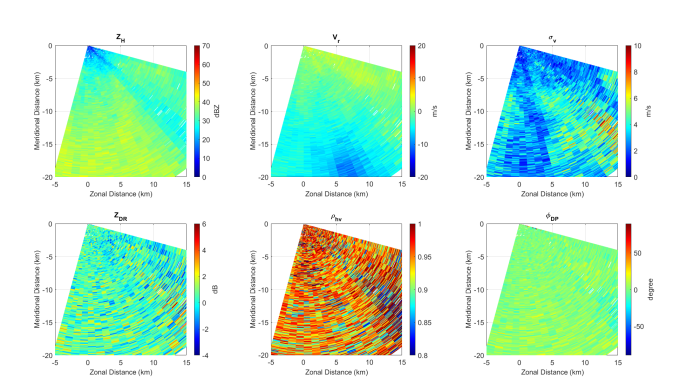


Fig. 16. Actual output images from CNN using 6 input variables of test case 2.

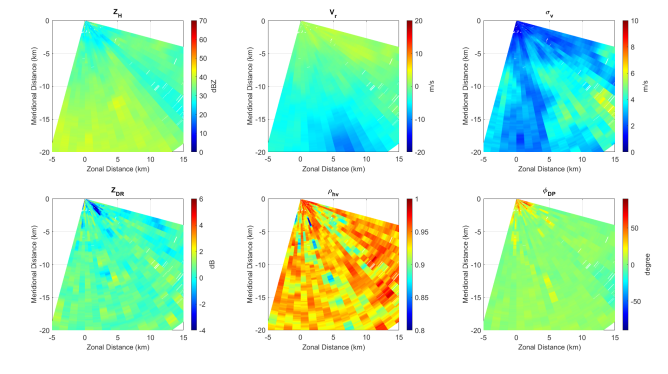


Fig. 20. Actual output images from speckle filter of test case 2.

z _H	V,	σ _v = 10
0 70	0	0
60	€ -5	€ -5
S .0	2 -9 10 10 10 10 10 10 10 10 10 10 10 10 10	8 2
A S Z Z Z	Se -10 0 12	18 -10 -10 -10 -10 -10 -10 -10 -10 -10 -10
20 C C C C C C C C C C C C C C C C C C C	10 0 2 E	6 (m)
20	30 - 15 - 10	15 - 15
10		
-20 5 0 5 10 15	-20	.20
-5 0 5 10 15 Zonal Distance (km)	-5 0 5 10 15 Zonal Distance (km)	-5 0 5 10 15 Zonal Distance (km)
Z	a a	4
2 _{DR} 6	0 Phv 1	φ _{DP}
· ·		
· ·		o degree
0 -5 -10 (Displace (hm)) 2 - 10 -10 (m) -10 ((w) 0.95	(in 4.5)
(a) do control to cont	0.00 0.00 0.00 0.00 0.00 0.00 0.00 0.0	(will controlled to the contro
2 gg 0		o degree

Fig. 17. Actual output images from CNN using 8 input variables of test case 1.

TABLE IV

RMSE OF CNN AND SPECKLE FILTER FOR TEST CASE 1

Radar Variables	CNN-6	CNN-8	Speckle filter
$Z_{\rm H}$ (dBZ)	1.61	1.48	4.51
$v_{\rm r}~({\rm m/s})$	1.04	1.01	2.17
$\sigma_{\rm v}~({\rm m/s})$	0.51	0.35	1.25
$Z_{\mathrm{DR}}\left(\mathrm{dB}\right)$	0.49	0.42	1.20
$ ho_{ m hv}$	0.036	0.023	0.132
$\phi_{\mathrm{DP}} (\mathrm{deg})$	5.34	3.27	18.59

 $TABLE\ V$ RMSE OF CNN AND SPECKLE FILTER FOR TEST CASE 2

Radar Variables	CNN-6	CNN-8	Speckle filter
$Z_{\rm H}$ (dBZ)	1.61	1.35	4.42
$v_{\rm r}~({\rm m/s})$	0.59	0.50	1.00
$\sigma_{\rm v}~({\rm m/s})$	0.30	0.18	0.82
$Z_{\mathrm{DR}}\left(\mathrm{dB}\right)$	0.42	0.30	1.11
$ ho_{ m hv}$	0.034	0.026	0.057
$\phi_{\mathrm{DP}} (\mathrm{deg})$	4.71	3.28	12.16

 $\label{table vi} TABLE\ VI$ LSTD of CNN and speckle filter for test case 1

Radar	LSTD of	LSTD of	LSTD of	LSTD of
Variables	CNN-6	CNN-8	speckle	ground
			filter	truth
$Z_{\rm H}$ (dBZ)	1.75	1.80	0.98	1.86
$v_{\rm r}~({\rm m/s})$	1.14	1.11	0.41	1.16
$\sigma_{\rm v}~({\rm m/s})$	0.88	0.93	0.24	0.93
$Z_{\mathrm{DR}}\left(\mathrm{dB}\right)$	0.58	0.57	0.15	0.54
$ ho_{ m hv}$	0.029	0.023	0.005	0.017
$\phi_{\mathrm{DP}}(\mathrm{deg})$	3.79	3.70	1.35	3.38

 $TABLE\ VII$ LSTD of CNN and speckle filter for test case 2

	TD OF CHILLIA	DI ECILEE I IE I E	CT OIC TEST CITS	
Radar	LSTD of	LSTD of	LSTD of	LSTD of
Variables	CNN-6	CNN-8	speckle	ground
			filter	truth
$Z_{\rm H}$ (dBZ)	1.53	1.55	0.40	1.62
$v_{\rm r}~({\rm m/s})$	0.82	0.77	0.18	0.82
$\sigma_{\rm v}~({\rm m/s})$	0.66	0.61	0.14	0.62
Z_{DR} (dB)	0.88	0.86	0.16	0.86
$ ho_{ m hv}$	0.041	0.036	0.007	0.038
$\phi_{\mathrm{DP}}(\mathrm{deg})$	5.48	5.94	1.20	5.84

V. SUMMARY AND CONCLUSION

In this paper, clutter detection and mitigation using machine learning approaches and physics-based discriminants are presented and evaluated. Actual measurements with the CPPAR show that CNN achieves the best clutter detection performance, followed by MLP and NBC. Additionally, the defined combination of power ratios and raw radar measurements is demonstrated to be more effective in clutter detection than the direct combination of raw radar measurements, and the physical explanations are provided. Furthermore, CNN is used for clutter mitigation and is shown to outperform the traditional speckle filter both qualitatively and quantitatively. Moreover, it is demonstrated that incorporation of power ratios in the training of CNN further improves its performance in clutter mitigation.

As in all other machine learning approaches, the performance of the three approaches examined here for clutter detection and mitigation depends on the representativeness and generalization of training datasets for testing cases. It is noted that there are still a few limitations and potential challenges of the discussed approaches. First, the training of the CNN is site specific and radar specific, that is, a different radar at another site may have a different nonlinear mapping relationship between the input variables and the output category, e.g., the learned weights of the CNN are probably different. In addition, compared to traditional clutter detection and mitigation methods, the computational cost of CNN-based approach during the training stage is higher, which usually demands powerful hardware

devices such as Graphics Processing Units (GPUs). Also, the data quality used for training and testing is very important. The sampling and estimation error as well as noise in radar measurements will negatively affect the accuracy of the learned model. All these factors pose potential challenges for the application of the CNN-based clutter detection and mitigation methods in real-world scenarios, which require further study and efforts to be addressed for a specific usage.

It has been shown that clutter detection and mitigation in polarimetric phased array radar measurements can be improved using CNN. This approach is also applicable to a mechanically scanned weather radar such as WSR-88D when the CNN is trained with the corresponding data that are representative for the weather scenarios, which is worthy of further study to improve the operational radar data quality.

Acknowledgment. The authors thank the staff engineers of the Advanced Radar Research Center (ARRC) at the University of Oklahoma for their dedication to the design and construction of the CPPAR system.

REFERENCES

- [1] P. Meischner, Weather Radar: Principles and Advanced Applications. New York: Springer, 2004.
- [2] J. C. Hubbert, M. Dixon, S. M. Ellis, and G. Meymaris, "Weather radar ground clutter. Part I: Identification, modeling, and simulation," *J. Atmos. Ocean. Technol.*, vol. 26, no. 7, pp. 1165–1180, Jul. 2009.
- [3] J. C. Hubbert, M. Dixon, and S. M. Ellis, "Weather radar ground clutter. Part II: Real-time identification and filtering," *J. Atmos. Ocean. Technol.*, vol. 26, no. 7, pp. 1181–1197, Jul. 2009.
- [4] Y. Li, G. Zhang, and R. J. Doivak, "Ground clutter detection using the statistical properties of signals received with a polarimetric radar," *IEEE Trans. Signal Process.*, vol. 62, no. 3, pp. 597–606, Feb. 2014.
- [5] Z. Li and G. Zhang, "Similarities and differences in clutter detection between electronic scans and mechanical scans with a polarimetricphased array radar," *IEEE Trans. Geosci. Remote Sens.*, doi: 10.1109/TGRS.2021.3063910.
- [6] G. Zhang, R. J. Doviak, D. S. Zrnić, R. D. Palmer, L. Lei, and Y. Al-Rashid, "Polarimetric phased-array radar for weather measurement: a planar or cylindrical configuration?" *J. Atmos. Ocean. Technol.*, vol. 28, no. 1, pp. 63–73, Jan. 2011.
- [7] Z. Li, G. Zhang, M.-H. Golbon-Haghighi, H. Saeidi-Manesh, M. Herndon, and H. Pan, "Initial observations with electronic and mechanical scans using a cylindrical polarimetric phased array radar," IEEE Geosci. Remote Sens. Lett., vol. 18, no. 2, pp. 271–275, Feb. 2021.
- [8] D. A. Warde and S. M. Torres, "The autocorrelation spectral density for Doppler-weather-radar signal analysis," *IEEE Trans. Geosci. Remote Sens.*, vol. 52, no. 1, pp. 508–518, Jan. 2014.
- [9] S. M. Torres and D. A. Warde, "Ground clutter mitigation for weather radars using the autocorrelation spectral density," *J. Atmos. Ocean. Technol.*, vol. 31, no. 10, pp. 2049–2066, Oct. 2014.
- [10] R. Vicen-Bueno, R. Carrasco-Álvarez, M. Rosa-Zurera, and J. C. Nieto-Borge, "Sea clutter reduction and target enhancement by neural networks

- in a marine radar system," Sensors, vol. 9, no. 3, pp. 1913–1936, Mar. 2009.
- [11] P. Jatau, V. Melnikov, and T.-Y. Yu, "A machine learning approach for classifying bird and insect radar echoes with S-band polarimetric weather radar," *J. Atmos. Ocean. Technol.*, vol. 38, no. 10, pp. 1797– 1812, Oct. 2021.
- [12] H. Kim and B. Cheong, "Robust velocity dealiasing for weather radar based on convolutional neural networks", *Remote Sens.*, vol. 15, no. 3, pp. 802, Jan. 2023.
- [13] M. S. Veillette, J. M. Kurdzo, P. M. Stepanian, J. McDonald, S. Samsi, and J. Y. N. Cho, "A deep learning-based velocity dealiasing algorithm derived from the WSR-88D open radar product generator", *Artificial Intelligence for the Earth Systems*, doi: 10.1175/AIES-D-22-0084.1.
- [14] G. Zhang, Weather Radar Polarimetry. Boca Raton: CRC Press, 2016.
- [15] I. Goodfellow, Y. Bengio, and A. Courville, *Deep Learning*. Cambridge, MA, USA: MIT Press, 2016.
- [16] MathWorks. *MATLAB Deep Learning Toolbox*. [Online]. Available: https://www.mathworks.com/products/deep-learning.html
- [17] J.-S. Lee, M. R. Grunes and G. de Grandi, "Polarimetric SAR speckle filtering and its implication for classification", *IEEE Trans. Geosci. Remote Sens.*, vol. 37, no. 5, pp. 2363-2373, Sep. 1999.
- [18] Q. Cao, G. Zhang, E. A. Brandes and T. J. Schuur, "Polarimetric radar rain estimation through retrieval of drop size distribution using a Bayesian approach", *J. Appl. Meteorol. Climatol.*, vol. 49, no. 5, pp. 973–990, May 2010.